ELSEVIER

Contents lists available at ScienceDirect

Materials & Design

journal homepage: www.elsevier.com/locate/matdes



Experimental investigations of the effectiveness of simultaneous topology/orientation optimization via SOMP and principal stress directions



Bailey Brown ^{a,*}, Nadim S. Hmeidat ^{b,c}, Xiu Jia ^a, Jackson Wilt ^b, Michael Roberts ^b, Brett G. Compton ^d, Natasha Vermaak ^a

- ^a Lehigh University, Mechanical Engineering & Mechanics, 19 Memorial Drive West, Bethlehem, PA 18015-3085, USA
- ^b Department of Mechanical, Aerospace and Biomedical Engineering, University of Tennessee, Knoxville, TN 37996, USA
- ^cUT Institute for Advanced Materials and Manufacturing (IAMM), University of Tennessee, Knoxville, TN 37920, USA
- d Department of Mechanical, Aerospace and Biomedical Engineering, Materials Science and Engineering Department, University of Tennessee, Knoxville, TN 37996, USA

HIGHLIGHTS

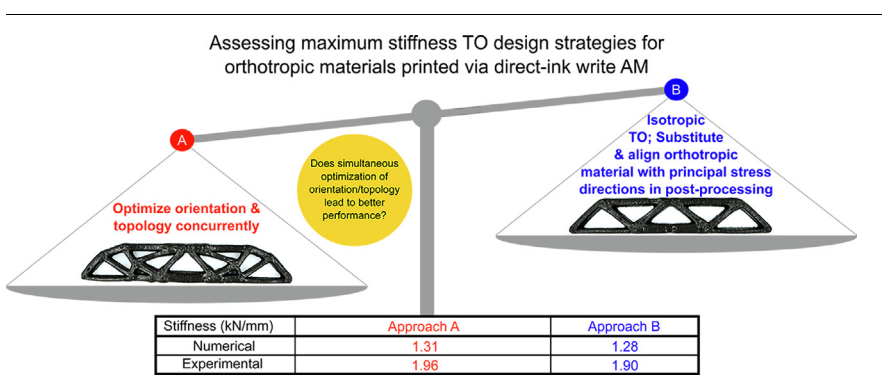
- Topology/orientation optimization with a principal stress approach is presented.
- Isotropic TO with orientations defined in post-processing was used for comparison.
- Optimized structures were printed via Direct-ink Writing with composite inks
- Microstructure imaging shows fibers align with contour-parallel deposition pattern.
- Equivalent performance was shown experimentally for examined design methodologies.

ARTICLE INFO

Article history: Received 23 December 2021 Revised 26 March 2022 Accepted 7 April 2022 Available online 15 April 2022

Keywords: Additive manufacturing Direct-ink write Orientation optimization Material anisotropy Topology optimization Composites

G R A P H I C A L A B S T R A C T



ABSTRACT

This article presents an analysis of simultaneous topology and orientation optimization based on a principal stress method within the Solid Orthotropic Material with Penalization (SOMP) framework. Numerical case studies were done to assess the expected benefits of including orientation in the design process for minimum compliance structures under single load cases printed with orthotropic materials. In particular, comparisons were made between structures designed with and without consideration of orthotropic material orientations during the topology optimization (TO) process. Direct-Ink Writing (DIW) additive manufacturing (AM) was used to print experimental specimens, which were tested in bending to validate numerical results. The novelty of the work centers on the experimental evaluation of the performance of optimized topologies designed with SOMP and manufactured via DIW. Additionally, new knowledge is presented in the form of corresponding numerical and physical experiments showing that with a principal-stress based material orientation updating scheme, equivalent performance can be achieved with respect to compliance by 1) optimizing topology and orientation concurrently with orthotropic material orientations controlled during TO using maximum in-plane principal stress directions; or 2) optimizing topology assuming equivalent isotropic properties, and substituting the original orthotropic properties along principal stress orientations post-optimization. This experimentally validated finding confirms that including orientation in the compliance-based design framework for AM of structures with orthotropic materials is not advantageous. For single load cases,

E-mail address: beb315@lehigh.edu (B. Brown).

^{*} Corresponding author.

using the standard Solid Isotropic Material with Penalization (SIMP) method for design purposes and then aligning material orientations with principal stress orientations after the design is produced is sufficient for obtaining equivalent performance benefits.

© 2022 The Authors. Published by Elsevier Ltd. This is an open access article under the CC BY-NC-ND license (http://creativecommons.org/licenses/by-nc-nd/4.0/).

1. Introduction

Topology optimization (TO) is continuing to exploit rapid advances made in additive manufacturing (AM) technologies. In particular, the complex and often organic-appearing shapes typically associated with optimized topologies are readily realizable via AM. However, the variety of AM approaches available also introduce their own challenges and features for the optimization process. As a result, much research has gone into tailoring TO protocols for additive manufacturing. Self-supporting [1–7], minimum feature size constraints [8,9], reduction of waste [10,11], optimization of infill and/or interior lattice structure [12–15], are some of the most critical aspects of TO for AM that have been widely investigated, among others [16].

An emerging trend in tailoring topology optimization for AM is the consideration of the directionality of material properties. It has been established that AM - specifically material extrusion AM results in anisotropic material properties. Moreover, inclusion of reinforcing fibers in the material extrusion AM of polymers has been shown to improve elastic properties, but with a strong dependence on the orientation of the fibers [17,18]. Material anisotropy has been shown to have a detrimental impact on TO when not accounted for in the optimization process [19,20]. Hmeidat et al. experimentally determined that print path resulted in a difference of up to 22% in the compliance objective function for benchmark optimized MBB beams printed in acrylonitrile butadiene styrene (ABS) using standard Fused Filament Fabrication (FFF) printing [19]. Chiu et al. reported that increasing the ratio of anisotropy in a material or the AM build direction angle has a negative impact on volume reduction achievable through TO [20]. Solid orthotropic material with penalization (SOMP) - a variation of the widely popular solid isotropic material with penalization (SIMP) densitybased TO method - has been investigated as a potential framework to develop topologies designed with optimal orientation for a given orthotropic material [21-25]. Many approaches to updating local material orientations have been examined. Some approaches for minimum compliance problems include direct optimization of the material orientation tensor [26,27] and optimization of weights on a sum of compliance tensors [28]. For additively manufactured composite materials, fiber orientations have also been optimized in parallel with topology by treating local printing speed as a design variable [29].

Another approach is based on the established principle that orthotropic materials offer the highest stiffness when aligned with principal strain or stress directions [30,31]. This can be taken advantage of by including material orientation in the finite element analysis (FEA) routine and simply updating orientation based on local principal stresses/strains. This method has been employed in a homogenization-based TO framework [32] and a bi-directional evolutionary structural optimization (BESO) TO framework [33,34]. While these design tools have been studied widely through numerical analysis, experimental validation of these emerging approaches and tailored TO approaches has been less extensive. In [35], Brooks and Moloney performed experimental analysis that quantifies the increase in strength obtained by reinforcing AM parts with reinforcing fibers aligned along paths informed by TO and principal stress orientations by using unreinforced parts as a point of comparison. Jiang et al. [21] showed that a SOMP/continuous fiber angle optimization (CFAO) framework yields stiffer structures when manufactured with contour-parallel deposition paths in comparison to structures designed and printed with fixed raster orientation angles of 0 and 90 degrees, respectively. Fernandes et al. [25] showed marked improvements in specific stiffness over traditional composite laminates for benchmark minimum compliance optimization problems as well as establishing the manufacturability of parts designed with SOMP and print paths planned using equally-spaced (EQS) or offset methods. Seifert et al. [29] demonstrated that printing speed can be used as a design variable controlling local orientation of fibers, and showed improvement over cases with a fixed print speed. Yang et. al. [36] showed the effect of build orientation on stiffness outcomes for structures printed with Stereolithography (SLA) and Selective Laser Melting (SLM).

Similar analysis has been performed on the subject of simultaneous versus sequential optimization of anisotropic material orientations and topology. Nomura et. al. [26,27] presented numerical case studies of sequential optimization (where they optimized the density, i.e. topology, assuming isotropic material properties and subsequently optimized the material orientation) compared to concurrent optimization, where orientation and density were optimized simultaneously. These optimization schemes, in contrast to the present work, were implemented directly on the Cartesian coordinates of the material orientation vector and tensor variables. For several single load case planar studies, Nomura et al. showed that the performance was comparable for both the concurrent and sequential optimization strategies (< 3% difference), while for multi-load cases (where a main principal stress direction can no longer be defined), they reported that concurrent optimization improved compliance performance by more than 5% [26]. To the best of the authors' knowledge, the current manuscript presents the first combined numerical and experimental study focusing on assessing the benefits of simultaneous topology/orientation optimization for orthotropic materials compared to simpler strategies.

In particular, the contribution of this paper lies in clarifying from an experimentally validated perspective - what benefit is obtained by considering orientation as a part of the single-load case design process (for example, in the minimum compliance design of AM structures) compared with simply aligning the print path with the principal stress orientations in post processing steps (i.e. to be concentric or approximately parallel with contours of the structure) and without requiring a sequential/secondary orientation optimization. The present article is the first to directly address this question. While in previous work, the performance of parts with optimized fiber orientations has been compared to composite laminates [29] and unidirectional prints [19,21], the current work compares the performance of a topology with simultaneously optimized fiber orientations/topology with a topology designed assuming equivalent isotropic properties, and substituting the original orthotropic properties along principal stress orientations post-optimization. This method of comparison offers a one-toone analysis and allows for a stronger conclusion to be drawn about the importance of considering orientation as an integral part of the topology optimization process. Additionally, this article expands on recent literature [19,21,25,29,35] illustrating and quantifying the challenges of translating designs obtained through

topology optimization to printed parts via AM. For example, realizing complex geometries often results in overfilling of regions within the structure, which significantly impacts mechanical behavior.

In designing for additive manufacturing with orthotropic materials through topology optimization, it is necessary to analyze how design choices practically impact performance. While it is known that aligning orthotropic materials along principal stress directions yields the optimal stiffness (or minimum compliance), an important question that remains is how the consideration of orientation during the design process affects the printed topology and performance. In other words, would similar benefits be physically observed by simply aligning materials with the principal stress orientation of the structure after the design has already been developed, or is it critically important to the printed structural performance to consider orientation during the optimization? In order to answer this question, it is necessary to isolate the effects of topological changes for a particular materials system and printing technique. This is achievable by making comparisons of topologies designed with and without consideration of orientation. Numerical analysis of the performance of these topologies with respect to the objective function (compliance) can yield insight into the theoretical impact of the inclusion of orientation during optimization. For example, previous purely numerical studies on the stiffness-based optimization of topology and orientation distributions for anisotropic composite materials have used cantilevers, bridges, MBB beams, and other structures under single and multiload cases [26,27] to demonstrate that the concurrent optimization is more beneficial for multi-load cases in planar design but yields non-negligible (5.7%) benefits for both single and multi-load cases when three-dimensional structures are examined [26]. However, in this article, experimental insight and validation are provided through a series of experiments using additively manufactured versions of topologies optimized using contrasting approaches. Two materials were selected for use in experiments: a carbonfiber (CF) reinforced epoxy ink (which exhibits orthotropic material properties) and a fumed silica (FS) reinforced epoxy ink (which exhibits nearly isotropic material properties).

In order to perform this analysis, an orthotropic finite element based SOMP topology and orientation optimization code was constructed and numerical case studies were conducted along with experimental evaluation. The TO framework is based on the example codes provided in Andreassen et al. and Ferrari et al. [37,38], along with finite element formulations for orthotropic materials [39]. For a select group of topologies that were optimized for minimum compliance, specimens were 3D-printed with Direct-Ink Writing (DIW) technology. Material characterization and flexural bending experiments were performed on these printed specimens.

The paper is organized as follows: Section 2 outlines the methods utilized in the numerical calculations and Section 3 gives the experimental set-up and procedures. Section 4 provides results of the numerical parametric studies. In Section 5 experimental results are presented: testing of DIW-produced topologies that were designed with 2 different approaches that isolates the effect of including orthotropic material orientations in the optimization process. Section 6 presents discussion of results and Section 7 summarizes relevant conclusions.

2. Numerical methods

TO is a powerful design method by which the optimal material distribution and connectivity within a design domain can be determined for given objectives, loading and boundary conditions, as well as constraints. It is a versatile tool that can be applied to a wide variety of optimization problems. Additionally, the principles of TO can be put into practice with a number of different

approaches, including homogenization, level sets, Bi-directional Evolutionary Structural Optimization (BESO), and Solid Isotropic Material with Penalization (SIMP). SIMP has emerged as one of the most commonly used TO protocols. While the standard SIMP protocol relies on the assumption of isotropic material properties, it is possible to extend SIMP to include orthotropic materials. This is often referred to as the Solid Orthotropic Material with Penalization (SOMP) method [21–24]. This framework is required in many situations when orthotropic materials are being used. Many AM processes produce materials with orthotropic material properties. Specifically, polymer material extrusion AM processes, such as Fused Filament Fabrication (FFF), Fused Deposition Modeling (FDM), and Direct Ink Writing (DIW) have been shown to produce materials with a significant degree of orthotropy [19,20,40-56]. Use of polymer material extrusion AM processes has become widespread in both academic research and industrial applications [57,58].

2.1. Problem formulation and solution schemes

As a case study, the commonly used benchmark example of compliance minimization of a MBB beam is examined:

$$\min_{\rho} \qquad U^{T} K(\tilde{\bar{\rho}}(\tilde{\rho}(\rho)), \theta) U \tag{1}$$

s.t.
$$K\left(\widetilde{\rho}\left(\widetilde{\rho}\left(\rho\right)\right),\theta\right)U=F;$$

$$\frac{\sum_{n} \stackrel{\sim}{\rho} \left(\stackrel{\sim}{\rho} \left(\rho \right) \right)_{n}}{n} = \nu_{f}; \quad 0 < \rho_{min} \leqslant \rho \le 1.$$
 (2)

In the objective function (Eq. 1), K is the global stiffness matrix, ρ is the design variable (relative density), $\tilde{\rho}$ is the density after filtering, $\bar{\rho}$ is the filtered, projected density, and U is the global displacement vector. In the constraints (Eq. 2), F is the global force vector, v_f is the volume fraction, n is the number of elements, and ρ_{min} is the minimum value for ρ ($\rho_{min}=10^{-6}$). Fig. 1 represents the design domain for half of the MBB beam (leveraging symmetry), where L is the beam half-length, and H is the height. The boundary conditions for the MBB beam are illustrated schematically at the top left corner (applied load, F) and bottom right corner (support). Based on a mesh convergence study (not shown) and resolution requirements for experimental design, a global mesh size of 450 \times 150 was adopted for all results in this manuscript.

The first step in developing a SOMP framework to perform TO on this benchmark problem, is to adopt an orthotropic FEA routine. One method for developing the stiffness matrices required for this FEA formulation is presented by Maki [39]. In the present work, Maki's method was extended to account for an arbitrary local material orientation θ (Fig. 2). Fig. 2 provides reference for local coordinates and orientation conventions for an element in the FEA mesh, utilized in the study.

In the SIMP method [59], FEA is used to determine sensitivities of the optimization objective function with respect to the design variable ρ (relative density). The relative density takes on a value $0<\rho_{min}\leqslant\rho\leqslant1$ for each element in the FEA mesh, where a value

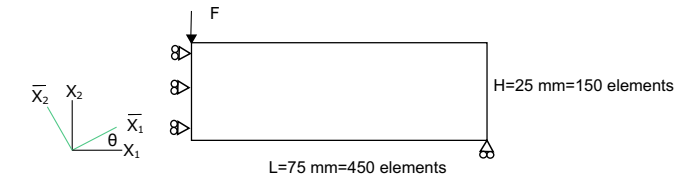


Fig. 1. Design domain and boundary conditions for half-symmetry MBB beam.

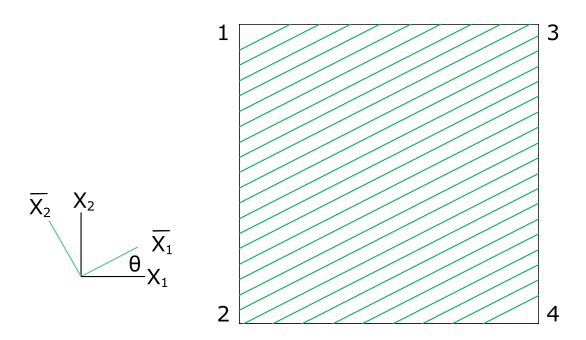


Fig. 2. 4-node rectangular element used in FEA.

of 1 represents solid material and a value of 0 represents void. The optimization process proceeds in an iterative manner until a convergence criterion is met (typically when the maximum change in relative density from the previous iteration falls below some threshold or a maximum number of iterations is reached). After convergence occurs, the relative densities of the mesh elements represent a material distribution of the optimized topology.

It has been shown that a viable method for determining optimal orientation for minimum compliance in orthotropic materials is to find the maximum (absolute value) in-plane principal stress direction [30]. The optimal orientation aligns the "stronger" material axis with the principal stress direction. An exception to this rule is the class of materials with relatively high shear stiffness (commonly called "shear strong" materials) that can be affected by the global repeated minimum problem [31]. If the material is *not* "shear strong" and the principal stress direction represents the optimal orientation, then:

$$\theta = \frac{1}{2} \arctan\left(\frac{2\sigma_{12}}{\sigma_{11} - \sigma_{22}}\right). \tag{3}$$

2.1.1. Solution schemes

To incorporate this concept in the SOMP framework for the present study, material orientations are updated iteratively along with elemental densities (see Fig. 3, left). At this step, θ will update to align with the principal stress direction for each element in the FEA mesh (modified if needed for "shear strong" materials). Introducing this updating of θ necessitates inclusion of a second FEA calculation prior to the sensitivity analysis. This additional step is required because the objective function and sensitivities are functions of the global displacement vector, U, which depends on θ (Eq. 1, Fig. 1). By recalculating the global displacement vector U after an orientation update (see Fig. 3, on the left), the sensitivities will be accurate for the current orientation and density field. Hereafter, this method will be referred to as the SOMP/PS Orientation Approach. It is readily apparent that the SOMP/PS method will be more computationally expensive than the traditional SIMP method, as additional calculations must be performed to optimize the local material orientations at each optimization iteration.

An alternate way to take advantage of the knowledge that principal stress-aligned orientations are optimal for compliance minimization is to utilize the less computationally costly SIMP Method, but augment it with a post-processing material alignment step. The protocol for this proposed method is presented in Fig. 3 (right). Hereafter, this method will be referred to as the *Modified SIMP* Approach. While this approach is less computationally costly, it will not capture information about orientation while the topology is being determined. It is therefore important to determine if the Modified SIMP Approach yields less optimal designs than the SOMP/PS Orientation Approach.

In this way, the SOMP/PS Orientation Approach and the Modified SIMP Approach are applied to the benchmark problem of the minimum compliance design of an MBB Beam (Fig. 1). The standard Method of Moving Asymptotes (MMA) [60] is applied to update the design variables in both the SOMP/PS Orientation Approach and the Modified SIMP Approach. The weighted averaging density filter from Andreassen et al. [37] is employed. This filtering technique creates a smoothed density field $\tilde{\rho}$ from the unfiltered density field ρ by employing a weighted average of the densities of adjacent elements within a certain radius. This filter provides an indirect measure of control over minimum feature size in the optimized topology as well as eliminates issues with mesh dependency and "checkerboarding" issues [59].

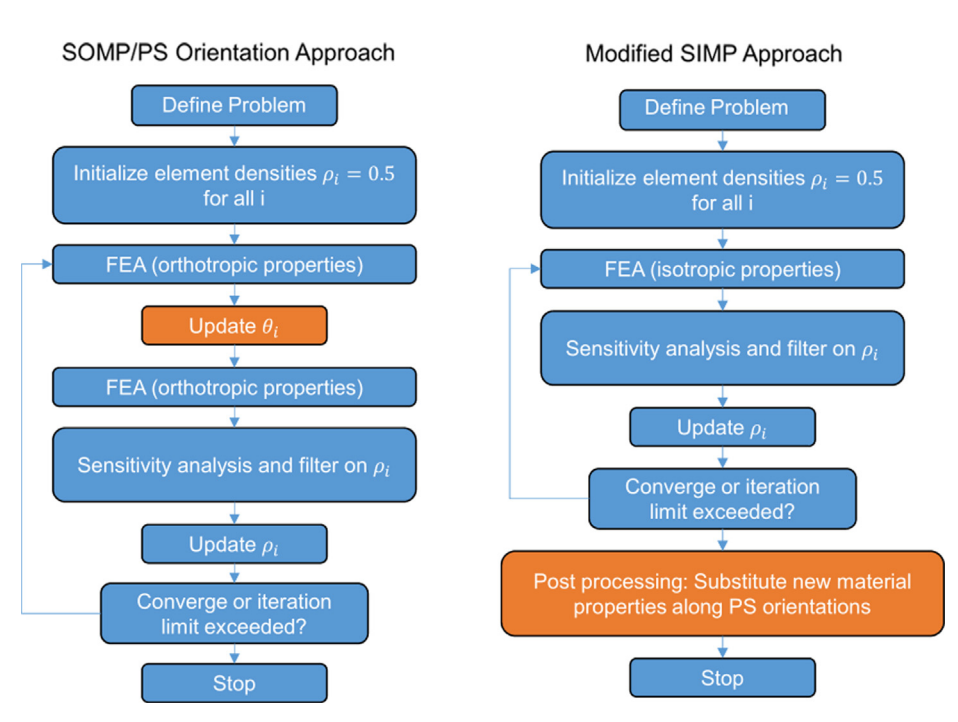


Fig. 3. Flow chart for SOMP/PS Orientation Approach (left) and Modified SIMP approach (right). Note that the subscript i refers to the ith element.

In conjunction with this filter, a modified Heaviside projection filter [61] is used to push intermediate density values towards 0 or 1, creating a black and white design which clearly delineates material and void regions. The function governing this projection is:

$$\bar{\tilde{\rho}} = \frac{\tanh(\beta\eta) + \tanh(\beta(\tilde{\rho} - \eta))}{\tanh(\beta\eta) + \tanh(\beta(1 - \eta))}, \tag{4}$$

where $\tilde{\rho}$ is the filtered density field and $\bar{\rho}$ is the filtered, projected density field, and β and η are parameters that control the sharpness and threshold of the projection, respectively [61]. The standard MMA algorithm [31,60] is augmented with the suggested changes provided by Guest et al. [62], which prevent oscillations and potential convergence issues associated with using a high value of β from the beginning of the optimization. According to Guest et al. [62], β can be assigned a constant, high value ($\beta \geq 20$). For the present work, $\beta = 40$ was chosen. Additionally, a value of $\eta = 0.5$ was selected and density variable ρ was uniformly initialized to coincide with the chosen value of η (Fig. 3). Finally, a fixed stopping criteria of 500 iterations was employed.

Material properties for the TO calculations were chosen to correspond with materials selected for the printing of experimental specimens - specifically, CF reinforced epoxy ink (which exhibits orthotropic material properties) and a FS reinforced epoxy ink (which exhibits nearly isotropic material properties). Comparisons were made with respect to minimum compliance (i.e. maximum stiffness) of structures designed with the SOMP/PS Orientation Approach and the Modified SIMP Approach, respectively. Specifically, a topology was designed using the Modified SIMP Approach with effectively isotropic material properties determined according to classical laminate theory. In particular, oriented plies made of carbon-fiber (CF) reinforced epoxy, with a [0,60,-60]s layup. (Note that a composite lay-up of [0/90/+45/-45]s could also have been chosen with identical resulting properties.) These isotropic properties are only used for the determination of the topology during the Modified SIMP optimization. The final calculation of stiffness for the numerical design (i.e. stiffness prediction) is performed in a post-processing step. Given the final optimal topology, the appropriate material properties (corresponding to either the CF reinforced epoxy or fumed silica (FS) reinforced epoxy) are substituted and the corresponding stiffness is determined. A second topology was designed using the SOMP/PS Orientation Approach and assuming the properties of the CF reinforced epoxy. Additional post-processing calculations of stiffness based on this final topology and orientation layout were made using the FS reinforced epoxy properties, for comparison. The results are presented in Section 4.

Because the Modified SIMP Approach is augmented with a postoptimization alignment of reinforced material with the maximum in-plane principal stress directions of the structure, the comparison with the SOMP/PS Orientation designed structure is direct in that the structures have the same material properties and orientation convention. However, the topologies are different due to the update of orthotropic material orientation during the design in the case of the SOMP/PS Orientation designed structure. This, therefore, provides a means by which to numerically quantify the difference in compliance provided by the differences in topology following related prior studies such as Nomura et. al. [27,26]. Again, the goal of the numerical predictions here is to make them specific to the materials systems and additive manufacturing technology of interest, to allow for detailed evaluation.

A numerical parametric study was also performed, based on the baseline CF reinforced epoxy, with varying degrees of directional dependence of the elastic stiffness (i.e. E_{22}/E_{11}). Comparing the SOMP/PS Orientation Approach and Modified SIMP Approach designed structures with varying E_{22}/E_{11} ratios provides insight

into whether consideration of orthotropy is more or less significant for different classes of materials. Some additional parameters - including volume fraction and shear modulus - were also investigated to determine their impact on the optimal topologies and stiffness for the SOMP/PS Orientation Approach and Modified SIMP Approach designed beams.

3. Experimental methods

3.1. DIW ink formulation

Epoxy-based inks were prepared for DIW. Two inks were formulated by adding filler materials that possess both anisotropic and isotropic morphologies (see Table 1). The first ink was formulated by initially mixing 5 g of DICY (Dicyanex 1400B, Evonik Industries AG, Essen, Germany) into 100 g of epoxy resin (Epon 826 Hexion Inc., Columbus, OH) using a centrifugal planetary SpeedMixer (FlackTeck, Inc., Landrun, SC) at 1800 rpm for 2 min. Next, 15 g (7.6 vol%; 11.4 wt%) of PAN-based chopped carbon fibers (CF) (AS4/BR102, Hexcel CO., Stamford, CT) were added and mixed for a total period of 12 min at 2000 rpm. The mixing period was divided into 3 min intervals. Each interval was followed by a rest period of 10 min to allow the ink and mixer to cool down. Next, 10 g (5.8 vol%; 7.6 wt%) of nanoclay (Garamite 7305, BYK Chemie GmbH, Wesel, Germany) was added in two steps. For each step, 5 g nanoclay was added and mixed at 2000 rpm for 3 min, followed by a rest period of 10 min. Next, the sides of the mixing container were scraped with a spatula, followed by another 3 min of mixing at 2000 rpm. Finally, 2 g (2.2 vol%; 1.5 wt%) of reactive diluent (EPODIL 748, Evonik Industries AG, Essen, Germany) was added to the final mixture and mixed at 2000 rpm for 2 min, to enable ease of extrusion. The final ink is referred to as the CF ink. The second ink was formulated by adding 11.65 g (5.6 vol%; 10 wt%) of isotropic fumed-silica (FS) (Cab-o-sil TS-720, Cabot Corporation, Alpharetta, GA) into the initial epoxy resin (100 g) and DICY (5 g) mixture. The amount of FS was added in two increments where the first half is added and mixed for 2 min at 1800 rpm and mixed again using the same parameters after adding the other half of FS. Finally, the sides of the mixing container were scraped with a spatula and the formulation was mixed for an additional 2 min at 1800 rpm. This ink is refereed to as the FS ink. All mixing steps were conducted under vacuum of 0.1 atm. The DICY is used in the inks as the latent curing agent for the epoxy resin, while the use of nanoclay or fumed silica is to impose sufficient shear thinning and yield stress behaviors that are critical for successful DIW 3D-printing [40,47,51–53,56,63,64]. The properties of the ink constituents are listed in Table 1.

3.2. 3D-printed composite specimens

After mixing, the resulting inks were loaded into 30 cc syringe barrels (Nordson EFD, Westlake, OH) using a spatula and

Table 1 Properties and morphology of ink constituents.

| Material | Morphology | Density (g/ cm³) |
|-----------------|--|---------------------|
| Epon 826 | Liquid | 1.16 |
| DICY | $<$ 10 μ m powder | 1.40 |
| CF | 7.1- μ m-diameter rods, 6 mm initial length | 1.79 |
| Nanoclay | \sim 6 μ m agglomerated platelets | 1.60 |
| Fumed silica | \sim 5–50 nm agglomerated spheroidal nanoparticles | 2.2 |
| EPODIL | Liquid | 0.86 |

centrifuged at 3900 rpm for 8 min using a Sorvall ST-8 Centrifuge (ThermoFisher Scientific, Waltham, MA) to get rid of any air bubbles that may have been introduced during the loading process, following [40,47,49]. The loaded syringe was then mounted on a 3-axis motion stage (Shopbot Tools, Inc, Durham, NC) equipped with a pneumatic extrusion system. Test samples were printed onto substrates covered with polytetrafluoroethylene (PTFE) coated aluminum foil (Bytac, Saint-Gobain Performance Plastics, Worcester, MA). A tapered metal luer-lock nozzle tip (S-type, GPD, Grand Junction, CO) with outlet diameter of 0.864 mm was used for deposition. All test samples were printed at a print speed of 20 mm/s using 50 psi extrusion pressure. The layer height and spacing between roads were set at 0.518 mm and 0.734 mm, respectively. The DIW process is illustrated schematically in Fig. 4a.

Rectangular flexural and shear test specimens were printed using two different print paths: (1) the longitudinal print path, in which printed roads were oriented parallel to the length of the specimen, and (2) the transverse print path, in which printed roads were oriented transverse to the length of the specimen. Print paths were programmed in g-code using Scilab software (Scilab Enterprises, Institut National de Recherche en Informatique et en Automatique, France). Following the printing process, all specimens were cured at 140°C for 24 h, followed by 2 h at 220°C. The printed flexural specimens had nominal dimensions of 65 mm \times 12.7 mm \times 3.2 mm following ASTM D790 [65], and shear specimens had nominal dimensions of 76 mm \times 19 mm \times 3 mm, following ASTM D5379 [66]. Edges of the printed specimens were ground smooth prior to testing. The v-notch was applied to the printed shear specimens via machining.

Topologically optimized structures were printed using both the CF and FS inks (Fig. 5). The structures were initially generated using the numerical optimization program to produce one half of the MBB flexural beams. Portable network graphic image files of the MBB beams were subsequently imported into a SolidWorks part file (Dassault Systemes, Vélizy-Villacoublay, France). The

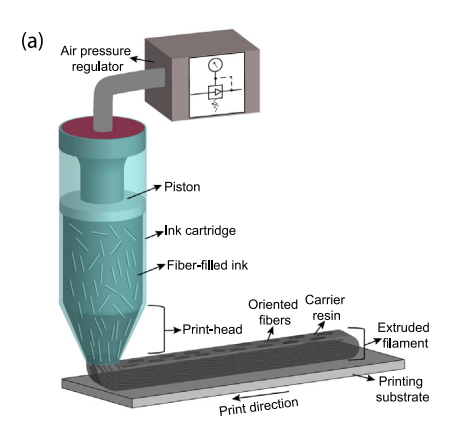




Fig. 4. (a) Schematic illustration of DIW of fiber composites, and (b) 3-point bending test setup.

images were then outlined using the internal add-on for Solid-Works called autotrace that enables an automatic sketch generation using the grey-scale pixelated images of the beams. Traced images for both the "isotropic topology" (topology designed with the Modified SIMP Approach for the FS reinforced epoxy) and "orthotropc topology" (topology/orientation designed with the SOMP/PS Orientation Approach for the CF reinforced epoxy) were then mirrored along their roller support edge and extruded to the desired thickness. The final testing geometry was 150 mm \times $40 \text{ mm} \times 15 \text{ mm}$. Each 3D beam was exported as an Stereolithography (STL) format file. The STL is then sliced or interpreted as gcode using the open-source printing software Ultimaker Cura 4.7 (Ultimaker, Utrecht, Netherlands). The chosen slicing algorithm results in a concentric print path, which is known to correspond well with the principal stress field used for the numerical design of the reinforced material directions. Optical micrographs of printed specimens were recorded using a VHX-5000 digital microscope (Keyence Corporation of America, Itasca, IL).

3.3. Mechanical characterization

All mechanical tests were performed at ambient temperature ($\sim 21^{\circ}\text{C}$). The printed CF and FS flexural specimens were tested in three-point configuration on an electromechanical load frame (Model 45, MTS Systems Corporation, Eden Prairie, MN, USA) using a load cell capacity of 10 kN, a span-length of 50 mm, and a crosshead speed of 1.3 mm/min for all tested specimens. Flexural properties are given in Tables 2 and 3 for both CF- and FS-based materials, respectively.

The topologically optimized, 3D-printed structures were tested in three-point bending on the aforementioned load frame and load cell. A support span of 145 mm (see Fig. 4b) and a cross-head speed of 1 mm/min were used for all printed structures. For each topology, three structures were 3D-printed and tested, and the load-deflection curves were recorded (Fig. 6 and Table 4).

In-plane shear tests were conducted on the v-notched printed shear specimens on a servohydraulic load frame (858 Table Top System, MTS Systems Corporation, Eden Prairie, MN, USA) using a 25 kN load cell and a cross-head speed of 2 mm/min. A 3D digital image correlation (DIC) system (Correlated Solutions, Inc) was used during the shear tests to measure shear strains.

The major Poisson's ratio of the CF printed composite, v_{12} , was calculated using the Rule-of-Mixture (ROM) correlation:

$$v_{12} = V_f v_{12f} + V_m v_m \tag{5}$$

where V_f is the volume fraction of the CF (0.076), v_{12f} is the major Poisson's ratio of the CF (0.2), V_m is the volume fraction of the matrix, and v_m is the Poisson's ratio of the matrix (0.347). With these values, $v_{12} = 0.335$ (Table 2). The FS epoxy ink is assumed to have the same Poisson's ratio as the epoxy matrix [67] (Table 3).

4. Numerical results

Before identifying optimal topologies to print and test and comparing numerical and experimental results, a number of parameters needed to be set and determined. For the following, a mesh size of 450×150 for the 3:1 aspect ratio half-beam (Fig. 1) was used. This choice was informed by a numerical sensitivity study (not shown) and the criteria that the resulting geometry be smooth enough to print. In addition, a filter radius of 15 was adopted, also based on a sensitivity study (not shown). All optimizations were stopped after 500 iterations. Below, further detail regarding the influence of shear modulus, degree of orthotropy, and volume fraction parameters on predicted stiffness is given. These parameter and property studies will provide context and insight for later

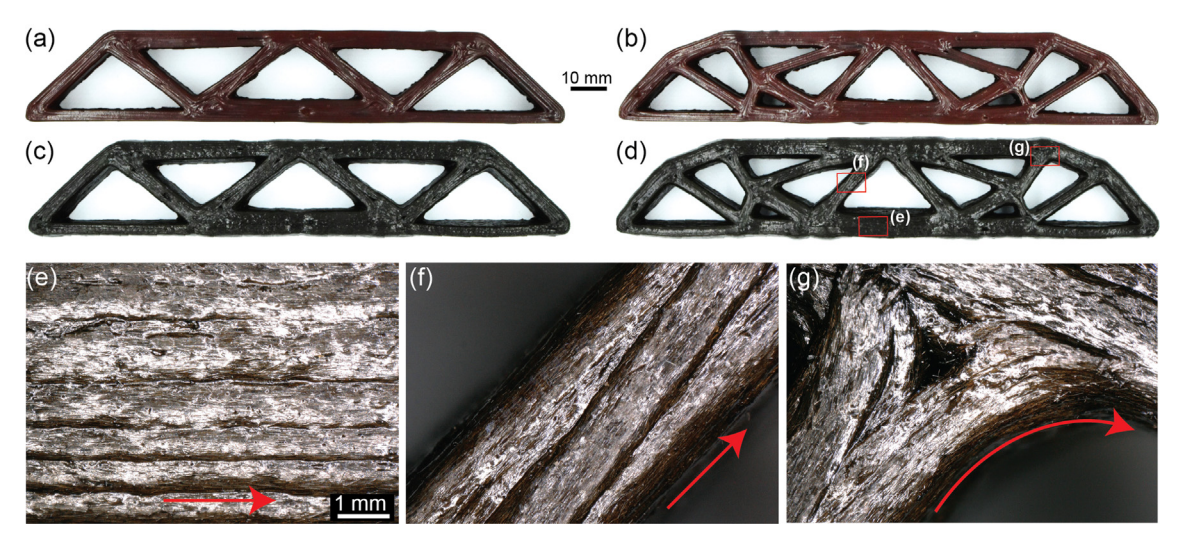


Fig. 5. Optical images of representative 3D printed topologically optimized geometries *before testing*: (a) FS "isotropic topology", (b) FS "orthotropic topology", (c) CF "isotropic topology", and (d) CF "orthotropic topology". (e - g) High-magnification optical micrographs for the regions highlighted by red boxes in (d), and red arrows indicate the translation direction of the deposition nozzle.

Table 2Mechanical properties of 3D printed CF reinforced epoxy coupons.

| Test direction | Flexure strength (MPa) | Flexure modulus (E_{11}, E_{22}) (GPa) | Shear strength (MPa) | Shear modulus (G_{12}, G_{21}) (GPa) | Poisson's ratio (v_{12} , v_{21}) |
|----------------------------|--|---|---|--|--|
| 1-direction 2-direction | $\begin{array}{c} 177.82 \pm 3.65 \\ 61.10 \pm 11.7 \end{array}$ | $\begin{array}{c} 10.1 \pm 0.43 \\ 3.71 \pm 0.29 \end{array}$ | $\begin{array}{c} 53.82 \pm 3.30 \\ 38.83 \pm 4.31 \end{array}$ | $\begin{array}{c} 2.11 \pm 0.27 \\ 1.43 \pm 0.034 \end{array}$ | 0.335 (v ₁₂) 0.123 (v ₂₁) |

Table 3 Mechanical properties of 3D printed FS reinforced epoxy coupons. Poisson's ratio ν is assumed to be equivalent to the epoxy matrix value. *Shear modulus is approximated based on the analytical expression for an isotropic material, $G = E/(2(1+\nu))$, where E is reported in the table as Flexure modulus.

| Test direction | Flexure strength (MPa) | Flexure modulus (E) (GPa) | Shear strength (MPa) | Shear modulus (G) (GPa) | Poisson's ratio (v) |
|----------------------------|---|---|----------------------|----------------------------|---------------------|
| 1-direction 2-direction | $\begin{array}{c} 109.2\pm2.98 \\ 110.6\pm3.76 \end{array}$ | $\begin{array}{c} 3.13\pm0.07 \\ 3.17\pm0.06 \end{array}$ | N/A N/A | 1.17* N/A | 0.35 0.35 |

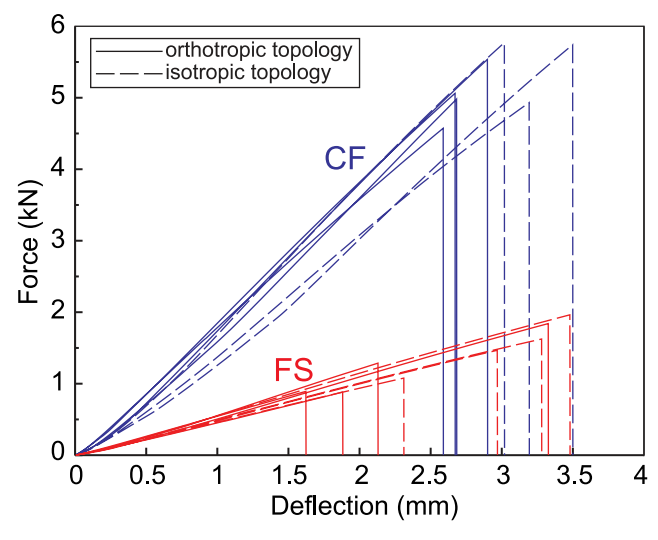


Fig. 6. Load-deflection curves for both the FS- and CF-based 3D printed structures.

discussion of results. As it was expected that the SOMP/PS Orientation Approach designed topology would have more complex features, the studies below were performed using this approach with CF reinforced epoxy material properties (Table 2).

4.1. Variation of shear modulus

The SOMP/PS Orientation Approach is expected to lead to the elastic moduli having an outsized impact on stiffness because of the elimination of shear stress in the principal stress configuration. As a result, the key numerical analysis below is focused on the elastic moduli - specifically, the relative magnitude of the elastic moduli E_{22} and E_{11} . However, it is important to verify that the impact of varying shear modulus (G_{12}) does not have a large contribution in changing topology and stiffness. This is especially true given that it is known that orientation of carbon fibers in reinforced polymers has an impact on measured in-plane shear modulus ([68]). To verify this, a numerical analysis was done in which 1-direction shear modulus G_{12} was varied by ± 2 GPa between the values of 0.11 GPa and 4.11 GPa. Note that the measured shear modulus (G_{12}) for the

Table 4Mechanical properties of FS- and CF-based 3D-printed topologically optimized structures.

| Property | FS (i) | FS (o) | CF (i) | CF (o) |
|-------------------------------|---------------|-----------------|---------------|---------------|
| Maximum load (kN) | 1.53 ± 0.40 | 1.22 ± 0.45 | 5.50 ± 0.48 | 5.04 ± 0.40 |
| Stiffness (kN/mm) | 0.52 ± 0.04 | 0.55 ± 0.05 | 1.90 ± 0.20 | 1.96 ± 0.10 |
| Mass (g) | 32.2 ± 2.40 | 35.1 ± 3.00 | 35.0 ± 2.8 | 39.4 ± 2.16 |
| Specific stiffness (kN/mm.kg) | 16.3 ± 0.30 | 15.7 ± 1.00 | 54.2 ± 2.5 | 50.0 ± 1.90 |

⁽i): isotropic topology; (o): orthotropic topology.

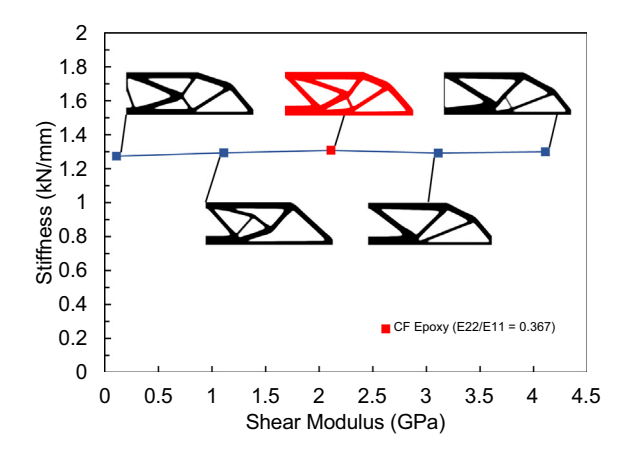


Fig. 7. Numerical predictions for stiffness of optimized MBB beams with varying shear modulus values.

CF reinforced epoxy was approximately 2.1 (Table 2). Stiffness values and topologies for select calculations are presented in Fig. 7.

The maximum predicted stiffness value is 1.31 kN/mm with a shear modulus of 2.11 GPa and the minimum predicted stiffness is 1.28 kN/mm with a shear modulus of 0.11 GPa. This represents a variation of 3.1% in stiffness. The results confirm the intuition that shear modulus variation would have little impact on the topology and stiffness for the orthotropic topology with materials aligned along principal stress orientations (Fig. 7). For the remainder of the analysis, shear modulus values (G_{12}) of 2.11 GPa (for CF reinforced epoxy cases) or 1.18 GPa (for FS reinforced epoxy cases) were employed (Tables 2, 3).

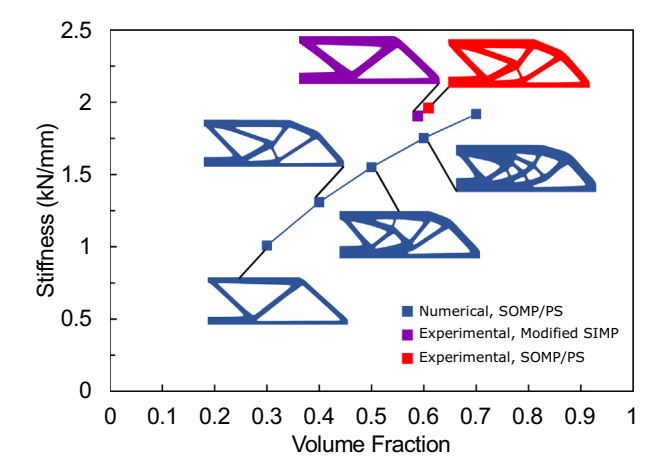


Fig. 8. Numerical predictions for stiffness of optimized MBB beams with varying volume fraction values. For reference, additional data points and topologies for experimentally measured stiffness and volume fraction values of the printed CF structures.

4.2. Variation of volume fraction

Volume fraction is easily controlled in a numerical design setting, but is less precisely controlled during manufacturing. This is especially true for additively manufactured structures with different topologies. Specifically, for the topologies that are printed for this study, one topology (designed using the Modified SIMP approach) has relatively simple features and another (designed using the SOMP/PS Orientation Approach) has relatively complex features. This could lead to some biasing of the measured stiffnesses of the structures due to disparate masses, despite the numerical designs having identical volume fractions. Because of this, it is of interest to investigate the impact of volume fraction variation on the predicted stiffnesses for the structures.

Fig. 8 presents topologies and predicted stiffness results from a study in which the volume fraction was varied from 0.3 to 0.7. All of the numerical results employed the SOMP/PS opimization approach for the CF reinforced epoxy. The maximum predicted stiffness value is 1.92 kN/mm with a volume fraction of 0.7 and the minimum predicted stiffness is 1.01 kN/mm with a volume fraction of 0.3. This represents a variation of 62.1% in stiffness. Experimental stiffnesses are also included for the CF reinforced epoxy specimens, with approximate volume fractions determined by scanning the topologies with ImageJ (Table 6). Note that the purple topology corresponds to the Modified SIMP Approach ("Isotropic Topology") and the red topology corresponds to the SOMP/ PS Orientation Approach ("Orthotropic Topology") as printed with CF epoxy. The volume fraction measured via ImageI for the experimental CF reinforced epoxy topologies were 52.5% (SOMP/PS Orientation Approach) and 47.5% (Modified SIMP Approach) larger than the numerically prescribed volume fraction (which was 0.4). As a result, experimentally measured stiffnesses for these cases were higher than the corresponding numerical predictions by

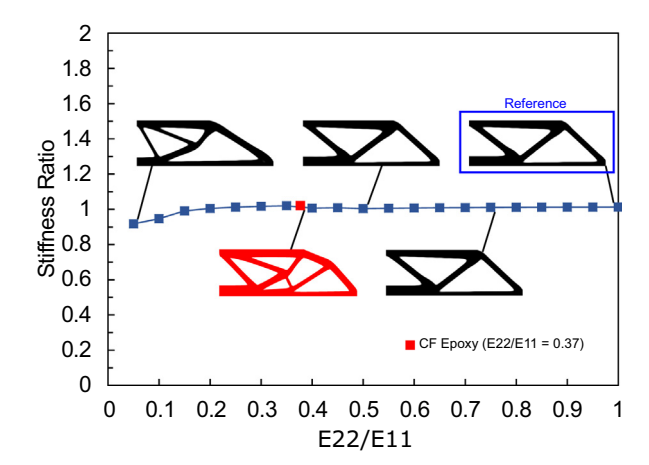


Fig. 9. Numerical predictions for stiffness of optimized MBB beams with varying ratios of orthotropic elastic moduli E_{22}/E_{11} . Red is used to denote results corresponding to the properties for the CF reinforced epoxy.

39.8% (SOMP/PS Orientation Approach) and 39.0% (Modified SIMP Approach). Further discussion is provided in Section 6.

4.3. Role of degree of orthotropy

A comparison was made between the numerical results for TO calculations performed with the SOMP/PS Orientation Approach and those with the Modified SIMP Approach. These comparisons were made over a range of orthotropy ratios (i.e. E_{22}/E_{11}) to determine trends that would be relevant for a wide range of orthotropic materials. The degree of orthotropy is a parameter that is also readily tunable with emerging techniques [56,69].

Fig. 9 shows normalized stiffness values and select topologies for calculations performed using the SOMP/PS Orientation Approach with a variety of E_{22}/E_{11} ratios from 0.05 to 1 in increments of 05). In particular, the higher elastic modulus E_{11} was fixed, reflecting the mechanical testing results for the CF reinforced epoxy ($E_{11} = 10.1$ GPa - Table 2). The modulus E_{22} was varied according to the given ratios plotted. The shear modulus (G_{12}) and Poisson's ratio (v_{12}) were kept constant at a value of 2.11 GPa and 0.335, respectively, to also be representative of the CF epoxy (Table 2). The normalized stiffness parameter ("Stiffness Ratio") is the stiffness for the SOMP/PS Orientation Approach designed topology with the given ratio E_{22}/E_{11} , along the x-axis, normalized by the stiffness for the Modified SIMP Approach designed topology using $E_{11} = E_{22} = 10.1$ GPa, i.e. $E_{22}/E_{11} = 1.0$, which is quasi-isotropic. The reference topology and stiffness at $E_{22}/E_{11} = 1.0$ is labeled in Fig. 9 at the right. This reference was chosen to help highlight performance trends based on the degree of orthotropy (related to E_{22}/E_{11}). Additionally, for comparison the case, $E_{22}/E_{11} = 0.37$, corresponding to the CF reinforced expoxy material of interest is denoted in red.

The material is the most orthotropic towards the left end of the figure, approaching $E_{22}/E_{11} = 0$. In the range $0 < E_{22}/E_{11} < 0.15$, there is an increase in predicted stiffness as the material becomes less orthotropic (E_{22}/E_{11} increases). In the range $0.15 < E_{22}/E_{11} \leqslant 1$, the stiffness remains largely constant as the material continues to become less orthotropic and approaches the quasi-isotropic reference case. For $E_{22}/E_{11} > 0.15$, the stiffness values varied by at most 1.5%. The maximum normalized stiffness value is 1.02 with a E_{22}/E_{11} ratio of 0.35 and the minimum normalized stiffness value is 0.92 with a E_{22}/E_{11} ratio of 0.05. Visual inspection of the topologies suggests that the orthotropic topology converges toward the quasi-isotropic topology for materials with higher E_{22}/E_{11} . Overall in Fig. 9, the stiffness ratio remains fairly constant over the entire range of E_{22}/E_{11} ratios considered. The implication is that the degree of orthotropy is not that significant for the beam compliance minimization problem as long as material orientation is aligned with principal stresses.

4.4. Numerical design of topologies to be experimentally tested

Based on the above studies and using a prescribed volume fraction of 0.4, and the orthotropy ratios E_{22}/E_{11} , representative of the CF material (Table 2, $E_{22}/E_{11} = 0.37$) or FS material (Table 3, $E_{22}/E_{11} \approx 1$), optimal topologies were determined using the two design strategies for orthotropic materials to be compared. These are (a) the SOMP/PS Orientation Approach using CF reinforced epoxy properties (b) Modified SIMP Approach using E = 6.35 GPa, v =.253, G = 2.53 GPa (corresponding to the effective isotropic properties of a [0, 60, -60]s laminate of CF reinforced epoxy). Note that topologies generated from topology optimization for isotropic materials are generally material agnostic (i.e. topology does not change based on magnitude of elastic modulus). Recall that for (b), post-processing steps are added: first the calculation for predicted stiffness is made by substituting the CF or FS reinforced

epoxy properties. Eventually the topology to be printed would also involve choosing a print path that aligns the material orientation with the principal stress directions (i.e., a concentric print path). Fig. 10 presents a comparison of the numerical results for these two strategies. The top images are the topologies, the middle images are the corresponding representations of the principal stress directions of the final design using sparse orientation vectors in blue. In the bottom row, the corresponding convergence histories are provided showing compliance as a function of optimization iterations. The predicted stiffness values for the respective topologies are presented in Table 5. The predicted stiffnesses were determined using the properties of the DIW printing materials to be used for experimental testing (the CF and FS inks, Tables 2, 3) and are listed according to the material indicated in the first column of Table 5.

These topologies were printed via the DIW process with a print path that closely approximates the numerically determined maximum in-plane principal stress field (i.e. a concentric, or contourparallel, print path). The experimental results (Section 5) therefore provide a validation check for the numerical findings, which is discussed in Section 6.

Based on the two topologies identified (i) "Orthotropic Topology" with variable orientation from the SOMP/PS Orientation Approach (Fig. 10a) and (ii) "Isotropic Topology" from the Modified SIMP Approach (Fig. 10b), additional numerical stiffness predictions were made for four scenarios with the two sets of material properties (CF Epoxy and FS Epoxy) and these are reported in Table 5. Given the "Orthotropic Topology" from the SOMP/PS Orientation Approach (Fig. 10a) and assuming the CF epoxy material properties, a stiffness of 1.31 kN/mm is predicted. For the same "Orthotropic Topology" from the SOMP/PS Orientation Approach (Fig. 10a), but instead substituting the (approximately isotropic) Fumed Silica epoxy material properties, a stiffness of 0.41 kN/ mm is calculated. Then considering the "Isotropic Topology" from the Modified SIMP Approach (Fig. 10b) and assuming the orthotropic CF epoxy material properties, a stiffness of 1.28 kN/mm is found. For the same "Isotropic Topology" from the Modified SIMP Approach (Fig. 10b) and instead substituting the (roughly isotropic) Fumed Silica epoxy material properties, 0.40 kN/mm is predicted. As seen in Table 5, there is a 3.1% variation in predicted stiffness between the two topologies using the CF epoxy properties, and a 2.5% difference in stiffness between the two topologies using the FS epoxy properties (Fig. 10a,b).

5. Experimental results

Table 2 summarizes the flexural and shear properties of the CF ink material. The CF ink exhibits directional dependence in both flexural modulus and strength, as compared to the isotropic flexural behavior achieved by the FS ink, which corroborates previous work by Hmeidat et al. [56]. The average flexural modulus and flexural strength values are 10.1 GPa and 177.82 MPa, respectively, for the longitudinal (i.e. 1-direction) CF specimens, and 3.71 GPa and 61.1 MPa, respectively, for the transverse (i.e. 2-direction) CF specimens. Directional dependence is also observed in the shear properties of the CF specimens. The average shear modulus and shear strength values are 2.11 GPa and 53.82 MPa for the longitudinal (i.e. 1-direction) CF specimens, and 1.43 GPa and 38.83 MPa for transverse (i.e. 2-direction) CF specimens, respectively.

Fig. 5 shows optical images of the topologically optimized, 3D printed structures using both the FS and CF inks. The FS ink results in printed, cured specimens with a characteristic brownish color (Fig. 5a-b), while the CF ink results in a black color (Fig. 5 c-d). Fig. 5e-g show high-magnification micrographs for the highlighted regions in Fig. 5d, demonstrating the preferred orientation of the

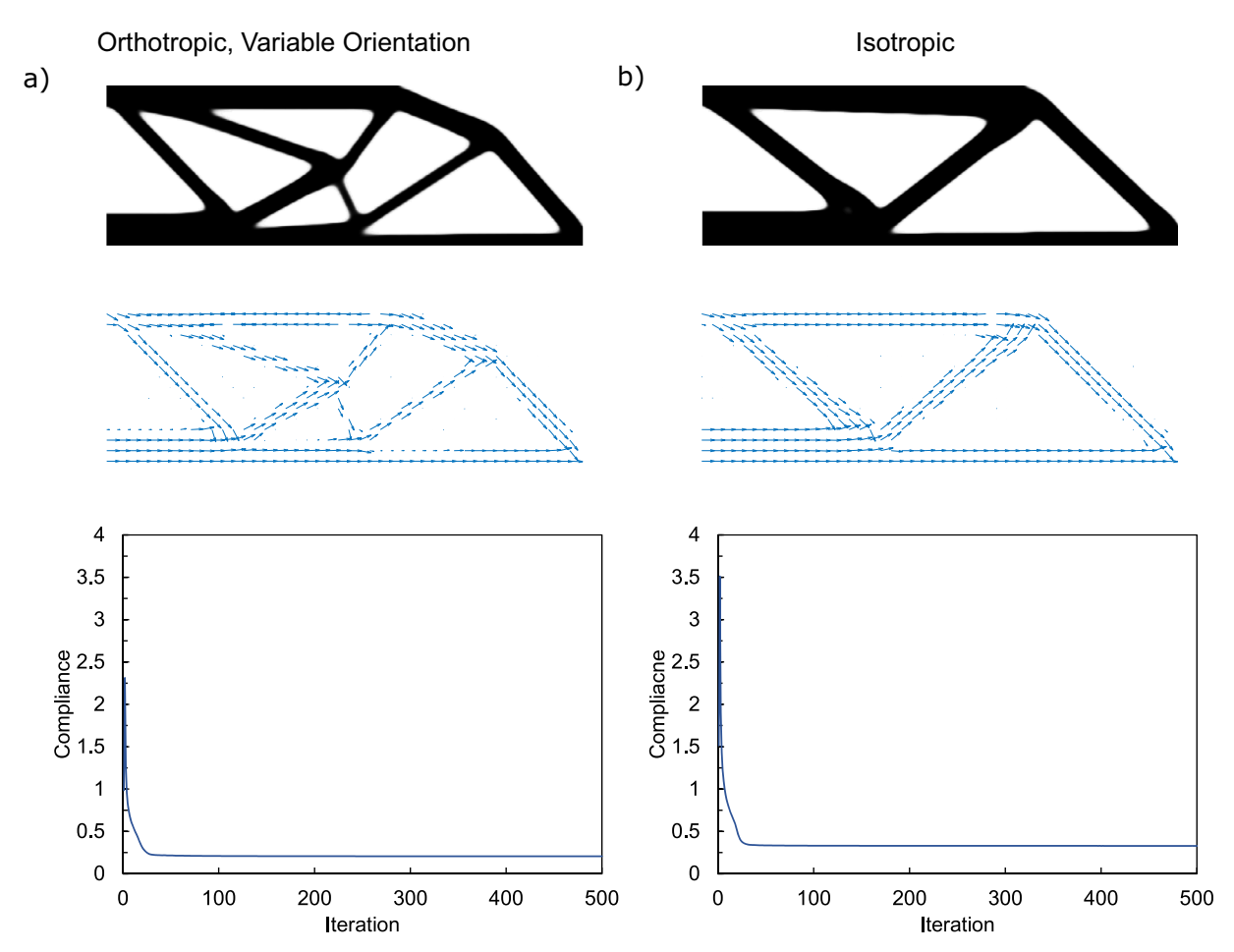


Fig. 10. Optimal topologies and local reinforced material orientation fields for the MBB beams using the a) SOMP/PS Orientation Approach and b) Modified SIMP Approach. Orientation vectors – shown as blue arrows – represent the principal stress directions of the final MBB design. Convergence histories for each topology are in the bottom row.

Table 5Stiffness values predicted by applying different sets of material properties to the "orthotropic" and "isotropic" topologies generated from the SOMP/PS and Modified SIMP Approaches, respectively.

| Material | "Orthotropic Topology" (from SOMP/PS Orientation Approach) | "Isotropic Topology" (from Modified SIMP Approach) |
|----------|--|---|
| CF Epoxy | 1.31 kN/mm | 1.28 kN/mm |
| FS Epoxy | 0.41 kN/mm | 0.40 kN/mm |

Table 6Measured volume fraction via imageJ for the two topologies printed with the two different materials.

| Ma | iterial | Measured volume fraction of printed "Orthotropic Topology" (from SOMP/PS Orientation Approach) | Measured volume fraction of printed "Isotropic Topology" (from Modified SIMP Approach) |
|----|---------|---|--|
| | Epoxy | 0.61 | 0.59 |
| 15 | Epoxy | 0.59 | 0.57 |

CFs along the translation direction of the deposition nozzle, as indicated by the red arrows.

The three-point bending setup for the printed structures is shown in Fig. 4b, and the corresponding force-deflection plots are given in Fig. 6. Table 4 summarizes the mechanical and physical properties of both the FS and CF structures. For the printed CF

Epoxy beams, a stiffness of 1.96 kN/mm was found for the "Orthotropic Topology" and a stiffness of 1.90 kN/mm was determined for the "Isotropic Topology". For the printed Fumed Silica beams, a stiffness of 0.55 kN/mm was measured for the "Orthotropic Topology" while a stiffness of 0.52 kN/mm was found for the "Isotropic Topology". The mean masses of the samples varied by 11.8% for the samples printed with CF Epoxy and by 8.6% for the samples printed with Fumed Silica. This is correlated with the difference in measured volume fraction. Using imageJ, the printed topologies were scanned to estimate volume fraction (Table 6). The mean measured volume fraction of the samples varied by 3.3% for the samples printed with CF Epoxy and by 3.4% for the samples printed with Fumed Silica.

Reflecting the dependence of stiffness on mass/volume of the topology, the specific stiffness values were calculated by scaling the respective stiffnesses by the mass of the corresponding beam. From an experimental perspective, this is the parameter that gives the most direct comparison in performance between the two topologies, as the disparity in mass is accounted for. For the printed CF Epoxy beams, a specific stiffness of 50.0 kN/mm.kg was observed for the "Orthotropic Topology" from the SOMP/PS Orientation design approach and a specific stiffness of 54.2 kN/mm.kg was determined for the "Isotropic Topology" from the Modified SIMP design approach. For the printed Fumed Silica beams, a specific stiffness of 15.7 kN/mm.kg was found for the "Orthotropic Topology" from the SOMP/PS Orientation design approach while a specific stiffness of 16.3 kN/mm.kg was measured for the "Isotropic Topology" from the Modified SIMP design approach. The mean

differences in specific stiffness for the topologies are 4.2 kN/mm.kg for the CF Epoxy printed beams and 0.6 kN/mm.kg for the Fumed Silica printed beams.

6. Discussion

As outlined in Section 4.2 and Section 5, one of the complicating factors in comparing the numerical and experimental results is the discrepancy between prescribed volume fraction (0.4) and the actual volume fraction of the printed specimens (Table 6). Nevertheless, the numerical study on the effect of prescribed volume fraction in Section 4.2 provides insight into how the stiffness should vary (up to 62.1% in the present study) given that the achieved volume fraction in the printed topologies is higher than what was set numerically. In general and as anticipated and shown in Fig. 8, volume fraction has a roughly linear correlation with predicted stiffness. While the numerical predictions for stiffness (Table 5) are not closely aligned with the measured stiffnesses of the experimentally tested printed specimens (Table 4), an adjustment must be made to account for the difference in mass/volume of the printed structures in comparison to the numerically prescribed volume fraction. As illustrated in Fig. 8, the experimentally measured stiffness values (in red and purple) match the numerically predicted values relatively well when compared with the measured volume fractions. In particular, when comparing the experimental stiffnesses of the CF epoxy structures for the "Orthotropic Topology" derived from the SOMP/PS approach (which had a measured volume fraction of 0.61) and the "Isotropic Topology" from the modified SIMP approach (with a measured volume fraction of 0.59) to the numerically predicted stiffness for the same respective volume fractions used in the parametric study (0.6), a difference of 10.8% (SOMP/PS) and 9.9% (Modified SIMP) is observed. In contrast, when comparing the experimental results to the numerically predicted stiffness for the intended volume fraction of 0.4, there is a difference of 39.8% ("Orthotropic Topology", SOMP/PS) and 39.0% ("Isotropic Topology", Modified SIMP), respectively. The increase in observed volume fraction of the printed structures due to error in printing will also have the effect of decreasing the magnitude of the stress in the structural members in comparison to what would be predicted numerically.

It is worthwhile to discuss the degree to which a concentric material deposition strategy approximates the principal stress orientations. For this purpose, the "Orthotropic Topology" design (SOMP/PS) is used as a reference. In Fig. 11, a colormap indicates

the local orientation for the principal stress direction (left) and the concentric g-code (right). The top row corresponds to the "Orthotropic Topology" and the bottom row corresponds to the "Isotropic Topology". The results show strong agreement between the two orientation fields for both topologies and suggest that this material deposition strategy is indeed an appropriate choice to approximate the numerically prescribed orientations.

In terms of the sources for the differences in printed volume fraction between the "Orthotropic Topology" from the SOMP/PS Orientation design approach and the "Isotropic Topology" from the Modified SIMP design approach, several factors contribute. For both materials, the printed "orthotropic topology" (SOMP/PS) had significantly greater volume fraction and was more massive than the printed "isotropic topology" (Modified SIMP). This is due to the increased complexity of the "orthotropic topology" leading to additional deposition of material, specifically at points in which the structural members of the design join together. Some progress has been made towards numerically addressing this issue and controlling joint feature size through two-step filtering, which may mitigate this problem [70]. While amongst the printed structures, the topology that ended up with the larger volume fraction ("Orthotropic Topology" from the SOMP/PS Orientation design approach) outperformed the topology that ended up with the smaller volume fraction ("Isotropic Topology" from the Modified SIMP design approach) with respect to stiffness for both the CF and FS epoxy materials (Tables 4), the opposite trend is observed with respect to specific stiffness. This indicates that the additional material present in the "Orthotropic Topology" (SOMP/PS) did not contribute to stiffness in proportion to its mass, i.e. this extra material was not used efficiently. This reinforces the need for more rigorous path planning with complex topologies, which is a highly active topic of current research [23,25].

However, statistical analysis of the specific stiffnesses of the beams allows for quantification of the significance of these findings. Based on the sample size and standard deviation of the sample population, it is possible to determine a p-value for the difference between the mean specific stiffnesses (\overline{S}) of the two topologies, $\overline{S}_{mod.SIMP} - \overline{S}_{SOMP/PS}$ (Table 4). For the CF reinforced epoxy printed beams, the p-value for the difference in mean specific stiffness is 0.188. For the FS reinforced epoxy printed beams, the p-value for the difference in mean specific stiffness is 0.378. The specific stiffnesses are therefore not statistically significant on a 0.05 significance level.

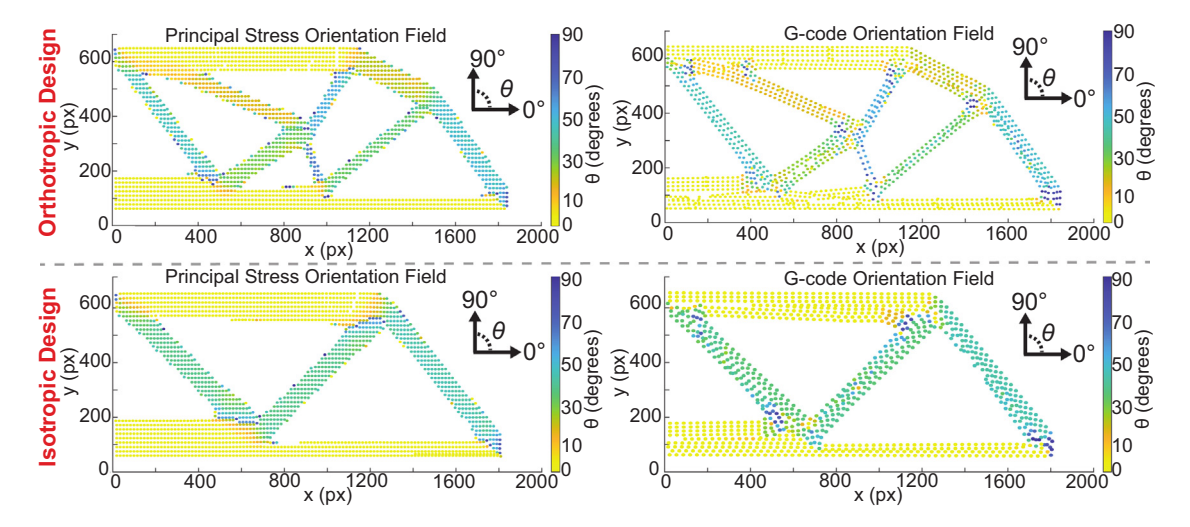


Fig. 11. The local orientation for the principal stress direction (left) and the concentric g-code (right) based on the SOMP/PS "Orthotropic Topology" design (top) and the Modified SIMP "Isotropic Topology" design (bottom).

Computationally, the Modified SIMP Approach is more efficient than the SOMP/PS Approach. The time taken to determine optimal topologies for 500 iterations was 4480 s for the SOMP/PS Orientation optimization and 3644 s for the Modified SIMP Approach optimization - a decrease of 19%. This disparity in computational cost can be exacerbated for problems that require a finer mesh, or if an extension to 3D is desired. Furthermore, the FEA routine utilized in both optimizations is not optimized for efficiency - specifically in the assembly of the stiffness matrix. Using the more efficient SIMP-based 88 line code ([37]) results in a topology that is essentially identical to the one produced in the Modified SIMP Approach, but has a much faster time of 846 s.

Given the added computational complexity and cost and the lack of statistically significant differences in stiffnesses experimentally measured (and numerically predicted) for the designs determined using the two strategies compared in this manuscript, the utility of concurrent topology and orientation optimization schemes is questioned. Other studies have addressed similar concerns. Nomura et. al. [26,27] investigated the benefit of concurrent orientation/topology optimization utilizing a sensitivity-based approach to optimize vector/tensor material orientation coordinates, concluding that the difference in minimum compliance design is marginal for single-load design cases but more significant for multi-load cases. Nevertheless, it should be emphasized that the work presented in this manuscript is novel in that it narrowly isolates the influence of considering material orientation concurrently with the TO of structures, specifically for DIW 3d-printing with orthotropic composite materials. Furthermore, to the best of the authors' knowledge, this is the first such study to also provide experimental validation. In this way, our findings add to the growing evidence that considering optimal orientation concurrently with TO is unneccessary for compliance-based single-load design cases.

7. Conclusions

The efficacy of the simultaneous optimization of topology and orthotropic material orientation (SOMP/PS Orientation Approach) for Direct-Ink-Write (DIW) additive manufacturing was evaluated for single load cases. For the first time, experimental results are combined with numerical predictions to confirm that differences in performance between structures designed with concurrent topology/orientation optimization (SOMP/PS) and those designed with simpler and less computationally costly approaches (Modified SIMP) are not statistically significant.

Experiments were performed on printed beams designed with the SOMP/PS Orientation Approach (orthotropic material orientations controlled during TO using maximum in-plane principal stress directions) and the Modified SIMP Approach (assuming equivalent isotropic properties, and substituting the original orthotropic properties along principal stress orientations postoptimization). Each beam was printed via DIW with a roughly isotropic material (a Fumed Silica reinforced epoxy) and a material with orthotropic behavior (a Carbon Fiber reinforced epoxy). The beams were printed with a concentric print path, which closely approximates the principal stress directions (which tend to follow the contour of a structure under mechanical loading). The results from this combined numerical and experimental study suggest that the most important factor in determining the performance of printed orthotropic structures is to align the strong axis of the material with the anticipated maximum principal stress directions. When using topology optimization to design such structures for additive manufacturing, it is less important to consider the orientation during the optimization process itself. This can be done with almost equal benefit, where benefit was evaluated experimentally, during post-processing with less numerical effort and complexity.

Data Availability

The raw/processed data required to reproduce these findings cannot be shared at this time as the data also forms part of an ongoing study.

Declaration of Competing Interest

The authors declare that they have no known competing financial interests or personal relationships that could have appeared to influence the work reported in this paper.

Acknowledgements

This material is based upon work supported by the United States National Science Foundation (NSF) under Grants #1825815, #11825437.

References

- Grégoire Allaire, Charles Dapogny, Rafael Estevez, Alexis Faure, Georgios Michailidis, Structural optimization under overhang constraints imposed by additive manufacturing technologies. J. Comput. Phys. 351 (2017) 295–328.
- [2] Weihong Zhang, Lu. Zhou, Topology optimization of self-supporting structures with polygon features for additive manufacturing, Comput. Methods Appl. Mech. Eng. 334 (2018) 56–78.
- [3] Martin Leary, Luigi Merli, Federico Torti, Maciej Mazur, Milan Brandt, Optimal topology for additive manufacture: A method for enabling additive manufacture of support-free optimal structures, Mater. Des. 63 (2014) 678– 690.
- [4] Matthijs Langelaar, Topology optimization of 3d self-supporting structures for additive manufacturing, Additive Manuf. 12 (2016) 60–70.
- [5] Andrew T Gaynor, James K Guest, Topology optimization considering overhang constraints: Eliminating sacrificial support material in additive manufacturing through design, Struct. Multidiscip. Optim. 54 (5) (2016) 1157–1172.
- [6] Amir M Mirzendehdel, Krishnan Suresh, Support structure constrained topology optimization for additive manufacturing, Comput. Aided Des. 81 (2016) 1–13.
- [7] Xu. Guo, Jianhua Zhou, Weisheng Zhang, Du. Zongliang, Chang Liu, Ying Liu, Self-supporting structure design in additive manufacturing through explicit topology optimization, Comput. Methods Appl. Mech. Eng. 323 (2017) 27–63.
- [8] D. Brackett, I. Ashcroft, R. Hague, Topology optimization for additive manufacturing, in: Proceedings of the Solid Freeform Fabrication Symposium, Austin, TX, vol. 1, 2011, pp. 348–362.
- [9] Boyan S Lazarov, Fengwen Wang, Ole Sigmund, Length scale and manufacturability in density-based topology optimization, Arch. Appl. Mech. 86 (1–2) (2016) 189–218.
- [10] Jingchao Jiang, Xu. Xun, Jonathan Stringer, Optimization of process planning for reducing material waste in extrusion based additive manufacturing, Robot. Comput.-Integrated Manuf. 59 (2019) 317–325.
- [11] Ruiliang Feng, Jingchao Jiang, Zhichao Sun, Atul Thakur, Xiangzhi Wei, A hybrid of genetic algorithm and particle swarm optimization for reducing material waste in extrusion-basedadditive manufacturing, Rapid Prototyping J. (2021).
- [12] Wu. Jun, Niels Aage, R\u00fcdiger Westermann, Ole Sigmund, Infill optimization for additive manufacturing-approaching bone-like porous structures, IEEE Trans. Visualization Comput. Graphics 24 (2) (2017) 1127-1140.
- [13] Anders Clausen, Niels Aage, Ole Sigmund, Exploiting additive manufacturing infill in topology optimization for improved buckling load, Engineering 2 (2) (2016) 250–257.
- [14] Wu. Jun, Anders Clausen, Ole Sigmund, Minimum compliance topology optimization of shell-infill composites for additive manufacturing, Comput. Methods Appl. Mech. Eng. 326 (2017) 358–375.
- [15] Lin Cheng, Jikai Liu, Albert C To, Concurrent lattice infill with feature evolution optimization for additive manufactured heat conduction design, Struct. Multidiscip. Optim. 58 (2) (2018) 511–535.
- [16] Jikai Liu, Andrew T. Gaynor, Shikui Chen, Zhan Kang, Krishnan Suresh, Akihiro Takezawa, Lei Li, Junji Kato, Jinyuan Tang, Charlie C.L. Wang, et al., Current and future trends in topology optimization for additive manufacturing. Struct. Multidiscip. Optim. 57 (6) (2018) 2457–2483.
- [17] M. Sugavaneswaran, G. Arumaikkannu, Modelling for randomly oriented multi material additive manufacturing component and its fabrication, Mater. Des. 1980–2015 (54) (2014) 779–785.
- [18] M. Sugavaneswaran, G. Arumaikkannu, Analytical and experimental investigation on elastic modulus of reinforced additive manufactured structure, Mater. Des. 1980–2015 (66) (2015) 29–36.
- [19] Nadim S Hmeidat, Bailey Brown, Xiu Jia, Natasha Vermaak, Brett Compton, Effects of infill patterns on the strength and stiffness of 3d printed topologically optimized geometries, Rapid Prototyping J. (2021).

- [20] Louis NS Chiu, Bernard Rolfe, Xinhua Wu, and Wenyi Yan. Effect of stiffness anisotropy on topology optimisation of additively manufactured structures, Eng. Struct. 171 (2018) 842–848.
- [21] Delin Jiang, Robert Hoglund, Douglas E. Smith, Continuous fiber angle topology optimization for polymer composite deposition additive manufacturing applications, Fibers 7(2) (2019b) 14.
- [22] Jonatan Rivilla Álamo, Francisco Ilson da Silva Júnior., Adapting the simp model for topology optimization of biomechanical structures, Pan American Congress of Applied Mechanics, 2012.
- [23] Vasileios S Papapetrou, Chitrang Patel, Ali Y Tamijani, Stiffness-based optimization framework for the topology and fiber paths of continuous fiber composites, Compos. Part B: Eng. 183 (2020) 107681.
- [24] Dustin R Jantos, Klaus Hackl, Philipp Junker, Topology optimization with anisotropic materials, including a filter to smooth fiber pathways, Struct. Multidiscip. Optim. (2020) 1–20.
- [25] Rossana R. Fernandes, Nekoda van de Werken, Pratik Koirala, Timothy Yap, Ali Y. Tamijani, Mehran Tehrani, Experimental investigation of additively manufactured continuous fiber reinforced composite parts with optimized topology and fiber paths, Additive Manufacturing, 2021, pp. 102056.
- [26] Tsuyoshi Nomura, Atsushi Kawamoto, Tsuguo Kondoh, Ercan M Dede, Jaewook Lee, Yuyang Song, and Noboru Kikuchi. Inverse design of structure and fiber orientation by means of topology optimization with tensor field variables, Compos. Part B: Eng. 176 (2019) 107187.
- [27] Tsuyoshi Nomura, Ercan M. Dede, Jaewook Lee, Shintaro Yamasaki, Tadayoshi Matsumori, Atsushi Kawamoto, Noboru Kikuchi, General topology optimization method with continuous and discrete orientation design using isoparametric projection, Int. J. Num. Methods Eng. 101(8) (2015) 571–605.
- [28] Yunfeng Luo, Wenjiong Chen, Shutian Liu, Quhao Li, Yaohui Ma, A discrete-continuous parameterization (dcp) for concurrent optimization of structural topologies and continuous material orientations. Compos. Struct. (2020) 111900
- [29] David Ryan Seifert, Andrew Abbott, Jeffery Baur, Topology and alignment optimization of additively manufactured, fiber-reinforced composites, Struct. Multidiscip. Optim. 63 (6) (2021) 2673–2683.
- [30] Pauli Pedersen, On optimal orientation of orthotropic materials, Struct. Optim. 1 (2) (1989) 101–106.
- [31] H.C. Gea, J.H. Luo, On the stress-based and strain-based methods for predicting optimal orientation of orthotropic materials, Struct. Multidiscip. Optim. 26 (3– 4) (2004) 229–234.
- [32] A.R. Diaz, MPe Bendsøe, Shape optimization of structures for multiple loading conditions using a homogenization method, Struct. Optim. 4(1) (1992) 17–22.
- [33] Xu. Liang, Gengdong Cheng, Two-scale concurrent topology optimization with multiple micro materials based on principal stress orientation, Struct.
- Multidiscip. Optim. 57 (5) (2018) 2093–2107.
 [34] Xiaolei Yan, Xu. Qiwang, Dengfeng Huang, Yong Zhong, Xiaodong Huang, Concurrent topology design of structures and materials with optimal material orientation, Compos. Struct. 220 (2019) 473–480.
- [35] Hadley Brooks, Samuel Molony, Design and evaluation of additively manufactured parts with three dimensional continuous fibre reinforcement, Mater. Des. 90 (2016) 276–283.
- [36] Kai Ke Yang, Ji Hong Zhu, Chuang Wang, Dong Sheng Jia, Long Long Song, Wei Hong Zhang, Experimental validation of 3d printed material behaviors and their influence on the structural topology design, Comput. Mech. 61(5) (2018) 581–598.
- [37] Erik Andreassen, Anders Clausen, Mattias Schevenels, Boyan S Lazarov, Ole Sigmund, Efficient topology optimization in matlab using 88 lines of code, Struct. Multidiscip. Optim. 43 (1) (2011) 1–16.
- [38] Federico Ferrari, Ole Sigmund, A new generation 99 line matlab code for compliance topology optimization and its extension to 3d. arXiv preprint arXiv:2005.05436, 2020.
- [39] A. Carl Maki, Finite Element Techniques for Orthotropic Plane Stress and Orthotropic Plate Analysis, volume 87. US Department of Agriculture, Forest Products Laboratory, 1968.
- [40] Brett G Compton, Jennifer A Lewis, 3d-printing of lightweight cellular composites, Adv. Mater. 26 (34) (2014) 5930–5935.
- [41] Nekoda van de Werken, Halil Tekinalp, Pouria Khanbolouki, Soydan Ozcan, Andrew Williams, Mehran Tehrani, Additively manufactured carbon fiberreinforced composites: State of the art and perspective, Additive Manuf. 31 (2020) 100962
- [42] A. Sydney Gladman, Elisabetta A Matsumoto, Ralph G Nuzzo, L. Mahadevan, Jennifer A Lewis, Biomimetic 4d printing, Nature Mater. 15 (4) (2016) 413– 418
- [43] Edward B Trigg, Nadim S Hmeidat, Louisa M Smieska, Arthur R Woll, Brett G Compton, Hilmar Koerner, Revealing filler morphology in 3d-printed thermoset nanocomposites by scanning microbeam x-ray scattering, Additive Manuf. 37 (2021) 101729.
- [44] Martin Spoerk, Chethan Savandaiah, Florian Arbeiter, Gerhard Traxler, Ludwig Cardon, Clemens Holzer, Janak Sapkota, Anisotropic properties of oriented short carbon fibre filled polypropylene parts fabricated by extrusion-based additive manufacturing, Compos. Part A: Appl. Sci. Manuf. 113 (2018) 95–104.
- [45] Vidya Kishore, Christine Ajinjeru, Andrzej Nycz, Brian Post, John Lindahl, Vlastimil Kunc, Ch.ad. Duty, Infrared preheating to improve interlayer strength

- of big area additive manufacturing (baam) components, Additive Manuf. 14 (2017) 7–12.
- [46] Halil L Tekinalp, Vlastimil Kunc, Gregorio M Velez-Garcia, Ch.ad.E. Duty, Lonnie J Love, Amit K Naskar, Craig A Blue, Soydan Ozcan, Highly oriented carbon fiber-polymer composites via additive manufacturing, Compos. Sci. Technol. 105 (2014) 144–150.
- [47] Nadim S Hmeidat, James W Kemp, Brett G Compton, High-strength epoxy nanocomposites for 3d printing, Compos. Sci. Technol. 160 (2018) 9–20.
- [48] Jiong Peng, Tung Liang Lin, Paul Calvert, Orientation effects in freeformed short-fiber composites, Compos. Part A: Appl. Sci. Manuf. 30 (2) (1999) 133–138
- [49] Nadim S Hmeidat, Daniel S Elkins, Hutchison R Peter, Vipin Kumar, Brett G Compton, Processing and mechanical characterization of short carbon fiber-reinforced epoxy composites for material extrusion additive manufacturing, Compos. Part B: Eng. 223 (2021) 109122.
- [50] Paul Calvert, Tung L Lin, Hogan Martin, Extrusion freeform fabrication of chopped-fibre reinforced composites, High Perform. Polym. 9 (4) (1997) 449– 456.
- [51] Nashat Nawafleh, Emrah Celik, Additive manufacturing of short fiber reinforced thermoset composites with unprecedented mechanical performance, Additive Manuf. 33 (2020) 101109.
- [52] Brett G Compton, Nadim S Hmeidat, Robert C Pack, Maximilian F Heres, Joshua R Sangoro, Electrical and mechanical properties of 3d-printed graphene-reinforced epoxy, Jom 70 (3) (2018) 292–297.
- [53] H.A. Pierson, E. Celik, A. Abbott, H. De Jarnette, L. Sierra Gutierrez, K. Johnson, H. Koerner, J.W. Baur, Mechanical properties of printed epoxy-carbon fiber composites, Exp. Mech. 59 (6) (2019) 843–857.
- [54] James P. Lewicki, Jennifer N. Rodriguez, Cheng Zhu, Marcus A. Worsley, Amanda S. Wu, Yuliya Kanarska, John D. Horn, Eric B. Duoss, Jason M. Ortega, William Elmer, et al., 3d-printing of meso-structurally ordered carbon fiber/ polymer composites with unprecedented orthotropic physical properties. Sci. Rep. 7 (1) (2017) 1–14.
- [55] Chad E. Duty, Vlastimil Kunc, Brett Compton, Brian Post, Donald Erdman, Rachel Smith, Randall Lind, Peter Lloyd, Lonnie Love, Structure and mechanical behavior of big area additive manufacturing (baam) materials. Rapid Prototyping J. (2017).
- [56] Nadim S Hmeidat, Robert C Pack, Samantha J Talley, Robert B Moore, Brett G Compton, Mechanical anisotropy in polymer composites produced by material extrusion additive manufacturing, Additive Manuf. 34 (2020) 101385.
- [57] Carmen M González-Henríquez, Mauricio A Sarabia-Vallejos, Juan Rodriguez-Hernandez, Polymers for additive manufacturing and 4d-printing: Materials, methodologies, and biomedical applications, Prog. Polym. Sci. 94 (2019) 57– 116.
- [58] Thomas Hofstätter, David Bue Pedersen, Guido Tosello, Hans Nørgaard Hansen, Applications of fiber-reinforced polymers in additive manufacturing, Procedia Cirp, 66 (Supplement C) (2017) 312–316.
- [59] Martin Philip Bendsoe, Ole Sigmund, Topology optimization: theory, methods, and applications, Springer Science & Business Media, 2013.
- [60] Krister Svanberg, The method of moving asymptotes—a new method for structural optimization, Int. J. Numerical Methods Eng. 24 (2) (1987) 359–373.
- [61] Fengwen Wang, Boyan Stefanov Lazarov, Ole Sigmund, On projection methods, convergence and robust formulations in topology optimization, Struct. Multidiscip. Optim. 43 (6) (2011) 767–784.
- [62] James K Guest, Alireza Asadpoure, Seung-Hyun Ha, Eliminating betacontinuation from heaviside projection and density filter algorithms, Struct. Multidiscip. Optim. 44 (4) (2011) 443–453.
- [63] Robert C Pack, Stian K Romberg, Aly A Badran, Nadim S Hmeidat, Trenton Yount, Brett G Compton, Carbon fiber and syntactic foam hybrid materials via core-shell material extrusion additive manufacturing, Adv. Mater. Technol. 5 (12) (2020) 2000731.
- [64] Brett G Compton, Jackson K Wilt, James W Kemp, Nadim S Hmeidat, Samantha R Maness, Mark Edmond, Steve Wilcenski, Jason Taylor, Mechanical and thermal properties of 3d-printed epoxy composites reinforced with boron nitride nanobarbs, MRS Commun. (2021) 1–6.
- [65] Inernational ASTM. Standard test methods for flexural properties of unreinforced and reinforced plastics and electrical insulating materials. ASTM D790-07, 2007.
- [66] ASTM Standard. D5379/d5379m, 2005, Standard Test Method for Shear Properties of Composite Materials by the V-Notched Beam Method. West Conshohocken, PA, 2005.
- [67] Lawrence E Nielsen, Generalized equation for the elastic moduli of composite materials, J. Appl. Phys. 41 (11) (1970) 4626–4627.
- [68] S. José Humberto, Almeida Jr, Clarissa C Angrizani, Edson C Botelho, Sandro C Amico, Effect of fiber orientation on the shear behavior of glass fiber/epoxy composites, Mater. Des. 1980–2015 (65) (2015) 789–795.
- [69] Jordan R. Raney, Brett G. Compton, Jochen Mueller, Thomas J. Ober, Kristina Shea, Jennifer A. Lewis, Rotational 3d printing of damage-tolerant composites with programmable mechanics. Proc. National Acad. Sci. 115(6) (2018) 1198– 1203.
- [70] Youngsuk Jung, Jaewook Lee, Seungjae Min, Multi-material topology optimization considering joint stiffness using a two-step filtering approach, Finite Elem. Anal. Des. 197 (2021) 103635.